Disintegration of ^{12}C, ^{19}F, ^{35}Cl, ^{63}Cu, and ^{65}Cu by real and virtual radiation

E. Wolynec, G. Moscati, J. R. Moreira, O. D. Gonçalves,* and M. N. Martins*
Instituto de Física da Universidade de São Paulo, São Paulo, Brazil
(Received 7 October 1974)

Yield curves were measured for one neutron emission in ^{12}C, ^{19}F, ^{35}Cl, and ^{65}Cu, and for two neutron emission in ^{63}Cu, with target stacks which were bombarded by electrons. The results were analyzed to compare the yields from the direct effect of the electrons with those resulting from bremsstrahlung from the electrons. The analysis was carried out with the virtual photon method in the plane-wave Born approximation and the distorted-wave Born approximation (DWBA). Agreement with DWBA predictions is obtained assuming photoabsorption through $E1$ transitions.

[NUCLEAR REACTIONS ^{12}C, ^{19}F, ^{35}Cl, ^{65}Cu; (γ, n), (e, e', n); ^{63}Cu, $(\gamma, 2n)$, $(e, e', 2n)$; $E = 16$–39 MeV; measured $\sigma_\gamma(E)/\sigma_e(E)$; DWBA virtual photon spectra analysis; deduced photoabsorption λ.]

I. INTRODUCTION

The direct interaction of the electromagnetic field of fast electrons with nuclear charges and currents is closely related to the interaction of photons with nuclei. When a photon is absorbed by a nucleus the momentum transfer is fixed by the photon energy, whereas when an electron transfers energy to a nucleus the momentum transfer has a continuous distribution. To the approximation that nuclear size can be neglected,[1] the relative effects of photons and electrons in producing nuclear reactions can be evaluated without detailed knowledge of nuclear wave functions. The only information needed is the multipole order of nuclear transitions involved. By relating the cross section for electron-nucleus excitation to the corresponding photoexcitation process, a virtual radiation spectrum can be defined[2]:

$$N^{(\lambda L)}(E_1, \omega)\frac{d\omega}{\omega} = \frac{\sigma_e^{\lambda}(L, E_1, \omega)}{\sigma_\gamma^{\lambda}(L, \omega)}, \tag{1}$$

where λ is the label either E or M for electric or magnetic transitions; L is the multipole order; σ_e is the cross section for electron-nucleus excitation (integrated over all scattering angles); σ_γ is the cross section for photon-nucleus excitation; ω is the photon energy (real and virtual); E_1 is the incident electron total energy; and $N^{(\lambda L)}$ is the virtual photon intensity spectrum.

From Eq. (1), the total inelastic electron scattering cross section may be expressed in a form similar to the yield in photoexcitation experiments:

$$\sigma_e(E_1) = \int_0^{E_1 - m_e} \frac{d\omega}{\omega} \sum_{\lambda L} \sigma_\gamma^{\lambda}(L, \omega) N^{(\lambda L)}(E_1, \omega). \tag{2}$$

Thus, expression (2) enables one to evaluate the electroexcitation cross section from the photoexcitation cross section $\sigma_\gamma^{\lambda}(L, \omega)$, if the virtual photon spectrum $N^{(\lambda L)}$ is known.

Using plane waves (PW) for the incoming and outgoing electrons, Thie, Mullin, and Guth[2] obtained expressions for $N^{(\lambda L)}(E_1, \omega)$ in the case of $E1$, $E2$, and $M1$ transitions:

For $E1$ the expression is

$$N_{\mathrm{PW}}^{E1}(E_1, \omega) = (\alpha/\pi)\{[(E_1^2 + E_2^2)/(E_1^2 - m_e^2)]\ln[(E_1E_2 + (E_1^2 - m_e^2)^{1/2}(E_2^2 - m_e^2)^{1/2} - m_e^2)/m_e\omega] - 2[(E_2^2 - m_e^2)/(E_1^2 - m_e^2)]^{1/2}\}, \tag{3}$$

where $E_2 = E_1 - \omega$, m_e is the electron's rest energy, and α is the fine structure constant. Using a distorted wave treatment (DW) with Dirac-Coulomb wave functions for the basis states of the electron, Gargaro and Onley,[3] obtained expressions for $N^{(\lambda L)}$ for all multipole orders:

$$N_{\mathrm{DW}}^{(\lambda L)}(E_1, \omega) = [(\alpha/\pi)(p_1/p_2)(E_1 + m_e)(E_2 + m_e)\omega^4(2L+1)^{-1}] \times \sum_{\kappa_1\kappa_2} S(\lambda)(2j_1+1)(2j_2+1)\,|C(j_1, j_2, L; -\tfrac{1}{2}, \tfrac{1}{2})R^{(\lambda)}(\kappa_1, L, \kappa_2)|^2, \tag{4}$$

where $p_1(p_2)$ is the initial (final) electron momentum; $S(\lambda)$ is the projection operator which retains only those terms satisfying the selection rules for electric or magnetic transitions of multipole order L; $j_1(j_2)$ is the initial (final) electron's total angular momentum; $\kappa_i = j_i + \frac{1}{2}$; and $R^{(\lambda)}$ involves a radial integral over electron's wave functions. The series solution to this integral is given in Ref. 3.

Experiments[4-8] comparing photodisintegration and electrodisintegration of nuclei have been reported. These experiments were carried out before the distorted wave treatment of virtual photon spectra[3] was available.

For light and medium weight nuclei the results of these experiments could be explained, in the plane wave approach, by assuming a mixture of $E1$ with up to 12% $E2$ contribution. For high Z the required $E2$ contribution was of the same magnitude or higher than the $E1$. A reanalysis of the above data with a distorted wave treatment[9] showed that they can be explained assuming only $E1$ transitions. For some of these experiments only three or four points were measured. The measurements near the threshold show, in general, disagreement with the predictions of both plane and distorted waves treatment.

With the aim of extending data to compare with the theoretical predictions, we carried out measurements of photodisintegration and electrodisintegration in some light and medium weight nuclei. The reactions studied were (a) one neutron emission from ^{12}C, ^{19}F, ^{35}Cl, and ^{65}Cu and (b) two neutron emission from ^{63}Cu.

II. MEASUREMENTS AND ANALYSIS

We used the three-foil stack method, for comparing the electrodisintegration and photodisintegration cross section, first described by Brown and Wilson.[4] In this method, a beam of monoenergetic electrons strikes, in succession a front target, a radiator for producing a known bremsstrahlung spectrum, and finally a back target as identical as possible to the front one. The foil thicknesses are chosen so that the activity N_1, in the front target, is mainly due to electrodisintegration, while that of the back, N_2, is caused by electrodisintegration and photodisintegration in approximately equal amounts. Neglecting the corrections due to the finite thickness of the stack the ratio of photodisintegration to electrodisintegration yields (Y_{Br}/Y_e) at the incident electron energy E_1 could be obtained directly by $(N_2 - N_1)/N_1$.

The electron beam was provided by the linear accelerator of the Instituto de Física da Universidade de São Paulo. The electron beam passed through a SEM (secondary emission monitor) before striking the targets placed in a vacuum chamber. For each bombardment the digitized SEM current was recorded in a multichannel analyzer operating in the time sequenced scaler mode (TSS)[10] so that accurate corrections for the decay during bombardments could be made.

The activities of the targets were measured by detecting in coincidence the energy-selected annihilation radiation in two NaI scintillation counters. The targets were often interchanged and counted in the same system. The coincidence pulses were stored in a multichannel analyzer operating in TSS, so that the desired initial activities could be obtained by analysis of the decay curves into their components.

For ^{12}C and ^{19}F we used Teflon (C_nF_{2n}) targets and for ^{35}Cl we used PVC (C_3H_5Cl) targets, which also furnished data on ^{12}C. For ^{63}Cu and ^{65}Cu we used natural copper targets. The radiator was ^{27}Al with a thickness of 0.546 g/cm^2 [2.28×10^{-2} radiation lengths (R.L.)]. The targets were typically 5×10^{-3} R.L. for PVC, 2×10^{-3} R.L. for Teflon and 5×10^{-3} R.L. for copper.

In correcting for the finite foil thickness we have used the method described by Barber[7]:

$$R_{\exp} = Y_{Br}/Y_e = R(E_1 - \tfrac{1}{2}\Delta_t) = R'\left[1 - R'\left(\frac{\frac{1}{2}t_t + t_f}{t_t + t_r}\right)\right]^{-1}, \tag{5}$$

where

$$R' = \left\{N_2(E_1)(1 - \tfrac{1}{2}\langle\theta^2\rangle) + \left[\frac{\partial(N_1(E_1) + N_2(E_1))}{\partial E_1}\right]\frac{(\Delta_t + \Delta_r)}{2} - N_1\right\}N_1^{-1}; \tag{6}$$

$N_1(E_1)$ is the activity (or yield) per electron induced in the first target foil; $N_2(E_1)$ is the activity (or yield) per electron in the target which is behind the radiator; t_t, t_r, and t_f are the thicknesses in radiation lengths of the target, radiator, and material upstream from the foil stack, respectively; Δ_t and Δ_r are the electron energy losses by radiation and collision in the target and radiator, respectively; and $\langle\theta^2\rangle$ is the mean square scattering angle of the electrons in the radiator.

In order to determine the correction term $D = \partial(N_1 + N_2)/\partial E_1$ a polynomial of degree n, $P_n(E_1)$ was adjusted to the experimental $(N_1 + N_2)$ data. Then, $D = P_n'(E_1) = dP_n(E_1)/dE_1$. The uncertainty in D was evaluated as

$$(\Delta D)_{\text{rms}} = \left[\sum_{i=1}^{n}\sum_{j=1}^{n}\frac{\partial P_n'}{\partial a_i}\frac{\partial P_n'}{\partial a_j}(H_{ij}^{-1})\right]^{1/2}, \tag{7}$$

where $P_n = \sum_{i=1}^{n+1} a_i x^{i-1}$ and H_{ij} is the error matrix for the coefficients of P_n'.

The n chosen was the one which gave the best χ^2 with a nonoscillatory solution for the fit. In all cases $2 < n < 4$.

III. RESULTS AND COMPARISON WITH THEORY

Figures 1 to 5 show the ratios of photodisintegration to electrodisintegration presented in units of $(Z_r^2 r_e^2 N_r)$, Z_r being the atomic number of the radiator, r_e the classical electron radius, and N_r is the number of atoms/cm^2 in the effective radiator.[11] In these units the ratios are called F and become independent of N_r.

The ratios predicted by theory are evaluated from

$$R_{\text{th}} = \frac{N_r \int_0^{E_1 - m_e} \sum_{\lambda L} \sigma_\gamma^\lambda(L, \omega) \phi(E_1, \omega, Z_r)(d\omega/\omega)}{\int_0^{E_1 - m_e} \sum_{\lambda L} \sigma_\gamma^\lambda(L, \omega) N^{(\lambda L)}(E_1, \omega)(d\omega/\omega)}, \tag{8}$$

where ϕ is the thin target bremsstrahlung spectrum produced in the effective radiator. In the present experiments, we have used the Schiff bremsstrahlung intensity spectrum for intermediate screening.[12]

In order to evaluate R_{th} we have to use measured values for $\sigma_\gamma^\lambda(L, \omega)$. However, $\sigma_\gamma^\lambda(L, \omega)$ is not an available experimental quantity. The available measurements give the total photo cross section $\sigma_\gamma(\omega) = \sum_{\lambda L} \sigma_\gamma^\lambda(L, \omega)$ without distinguishing the different multipolarities. If it is possible to assert that one multipole is dominant (usually $E1$), then the sum in Eqs. (2) and (8) reduces to a single term. In such cases, the electrodisintegration cross section should be exactly predictable from the photodisintegration cross section. If this is not the case then electrodisintegration can conceivably be used to detect the contribution of quadrupole or other multipolarities in the photo cross section. As shown in Refs. 3 and 13 the quadrupole component of the virtual photon spectra, in the distorted wave calculation, is one order of magnitude bigger than the dipole. In contrast, real radiation is a plane wave and the plane wave contains all multipole components in equal amounts.

In the previously reported experiments on the ratio of photodisintegration to electrodisintegration[4-8] the measured σ_γ were assumed to be

$$\sigma_\gamma(\omega) = \alpha \sigma_\gamma^E(1, \omega) + \beta \sigma_\gamma^E(2, \omega) \tag{9}$$

with α and β constants, determined by fitting expression (8) to the experimental data, and using $N^{\lambda L}$ evaluated in the plane wave approximation.

It is our purpose to show that, if Coulomb distortion is taken into account, there is no need to invoke large amounts of $E2$ contribution to explain experimental data. We then assume for the present, that the measured photo cross sections were entirely due to electric dipole absorption.

The curves labeled F_{PW} and F_{DW} in Figs. 1 to 5 were evaluated from the expressions:

$$F_{\text{PW}}^{(E1)} = (N_r / Z_r^2 r_e^2 N_r) \times \frac{\int_0^{E_1 - m_e} \sigma_\gamma(\omega) \phi(E_1, \omega, Z_r)(d\omega/\omega)}{\int_0^{E_1 - m_e} \sigma_\gamma(\omega) N_{\text{PW}}^{E1}(E_1, \omega)(d\omega/\omega)}, \tag{10}$$

$$F_{\text{DW}}^{(E1)} = (N_r / Z_r^2 r_e^2 N_r) \times \frac{\int_0^{E_1 - m_e} \sigma_\gamma(\omega) \phi(E_1, \omega, Z_r)(d\omega/\omega)}{\int_0^{E_1 - m_e} \sigma_\gamma(\omega) N_{\text{DW}}^{E1}(E_1, \omega, Z_t)(d\omega/\omega)}, \tag{11}$$

where N_{PW}^{E1} is given in expression (3), σ_γ is the measured photodisintegration cross section, and N_{DW}^{E1} is given by an analytical expression[13] which fits the calculations of Gargaro and Onley[3] for $\lambda = E$ and $L = 1$:

$$N_{\text{DW}}^{E1}(E_1, \omega, Z_t) = N_{\text{PW}}^{E1}(E_1, \omega) + \omega[1.29 \times 10^{-5} \exp(1.245 Z_t^{1/3} - 0.052 E_1)]\,(E_2 + m_e)/(E_1 + m_e), \tag{12}$$

where Z_t is the target atomic number. In evaluating expressions (10) and (11) we have used, for σ_γ, data available in the literature.[14-17]

The errors of experimental points shown in Figs. 1 to 5 include (a) the uncertainty in the initial activities obtained by standard statistical methods; (b) the uncertainty in the correction term D, evaluated as described in Sec. II; and (c) an estimative of the fluctuations of the SEM. The largest contribution to the total error comes from the uncertainty in D. For a few points near threshold the uncertainty in D was as high as 100%, decreasing typically to about 10% in the steep part of the yield curve.

In all figures the χ^2 values are per degree of freedom. The dashed curves are the result of a polynomial fit to experimental data. The small values of χ^2 for this fit are indicative that the cri-

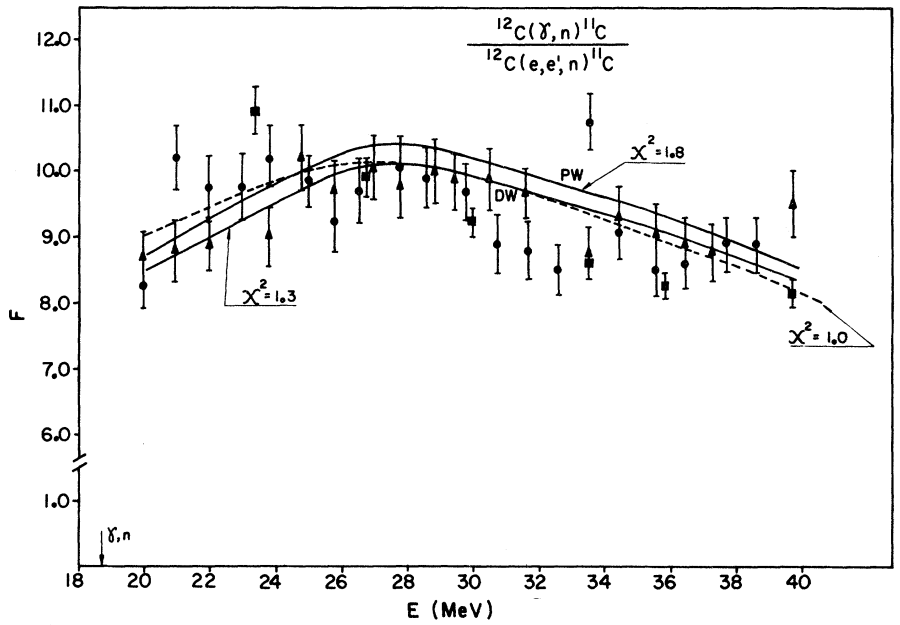

FIG. 1. Measured F for $^{12}C(\gamma, n)$. The full circles and triangles refer to our measurements with Teflon and PVC targets, respectively. Full squares are data from Ref. 7. Dashed curve is a polynomial fit to the points. Full curves are F_{PW} and F_{DW} predictions.

teria adopted to evaluate the derivative of the yield curve $(N_1 + N_2)$ leads to an overestimate of the total error. However, we found no other systematic way of evaluating this derivative with its uncertainty.

For ^{12}C, Fig. 1, F_{PW} and F_{DW} are almost the same, and experimental data are compatible with both. For the other nuclei studied, Figs. 2 to 5, experimental data are in good agreement with the distorted wave predictions for electric dipole transitions. This can be seen by the χ^2 values of the DW curves, which reflect how well the theoretical predictions fit the measured points (no free parameters adjusted).

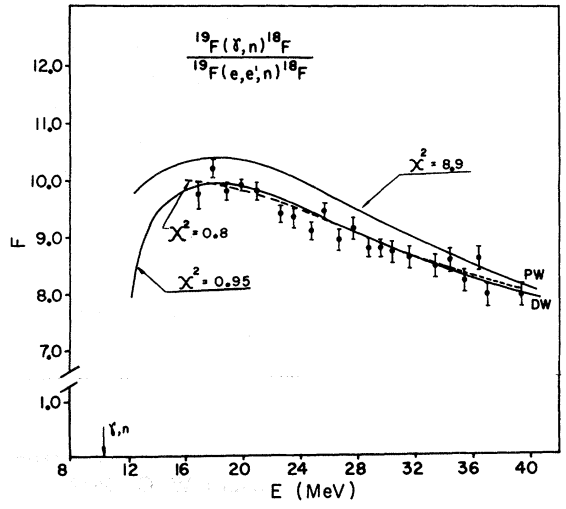

FIG. 2. Measured F for $^{19}F(\gamma, n)$. Dashed curve is a polynomial fit to the points. Full curves are F_{PW} and F_{DW} predictions.

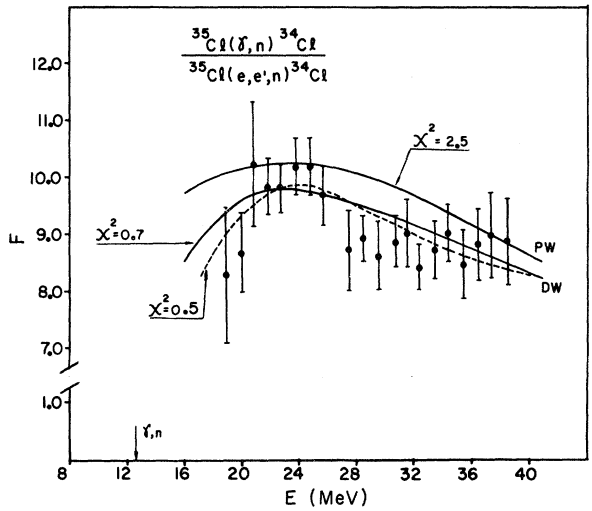

FIG. 3. Measured F for $^{35}Cl(\gamma, n)$. Dashed curve is a polynomial fit to the points. Full curves are F_{PW} and F_{DW} predictions.

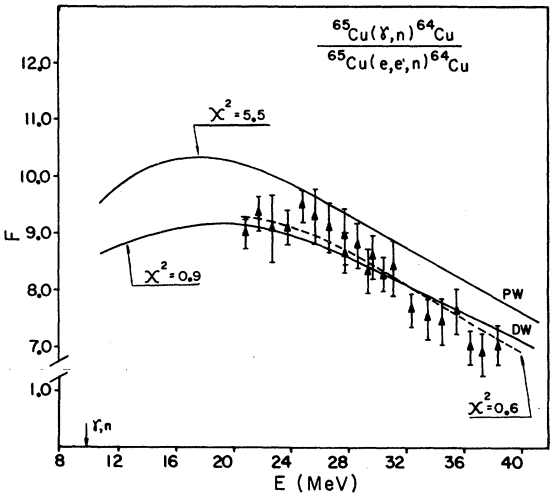

FIG. 4. Measured F for $^{65}Cu(\gamma, n)$. Dashed curve is a polynomial fit to the points. Full curves are F_{PW} and F_{DW} predictions.

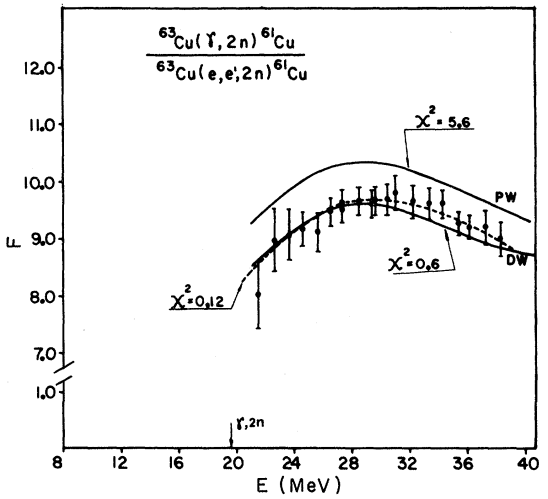

FIG. 5. Measured F for $^{63}Cu(\gamma, 2n)$. Dashed curve is a polynomial fit to the points. Full curves are F_{PW} and F_{DW} predictions.

IV. CONCLUSIONS

Previously published data[4-8] on the ratio of photodisintegration to electrodisintegration analyzed in the virtual photon method, using plane wave approximation suggested the need to assume large amounts of $E2$ contribution in order to explain experimental data. Recently a reanalysis of these data, taking into account Coulomb distortion[9] and assuming only $E1$ transitions, showed agreement between theory and experiment, within experimental errors, apart from data near threshold. The disagreement near threshold was suggested to be due to unreliable corrections for energy degradation of the electrons, which become important in this region.

From the present measurements and its analysis we can conclude that the distorted wave calculation, based on the formalism of Gargaro and Onley,[3] explains the experimental data assuming only $E1$ transitions, even near threshold.

An estimate of the strength of $E2$ transitions, compatible with our results depends on the location of the $E2$ resonance. If we assume a quadrupole resonance located around $58A^{-1/3}$ MeV, as suggested by Bohr and Mottelson,[18] then our data are compatible with an $E2$ resonance in the photo cross section, having an integrated cross section of up to 2% of the $E1$ resonance integrated cross section.

We would like to comment on the existence of an $E2$ giant resonance. Several measurements[19-24] have been reported on the detection of an $E2$ or $E0$ resonance. In these measurements the $E2$ or $E0$ resonance was detected by looking to the (e, e') or (p, p') cross sections at a particular scattering angle and choosing a suitable momentum transfer, in order to enhance quadrupole compared to dipole. In our experiment we measured the cross section integrated over all scattering angles and in this case the quadrupole contribution becomes negligible, when compared with the dipole one.

From the theoretical point of view we can evaluate, as an example, the predicted ratio between the $E2$ and $E1$ integrated photoabsorption cross sections, for ^{12}C, using sum rules. We have used the isoscalar energy weighted sum rule[25] for the $E2$ transitions and expression (47) of Ref. 26 for the $E1$. The value obtained for the $E2$ integrated photoabsorption cross section is 1.3% of the $E1$.

Recent measurement[27] of the total cross section for the electrofission of ^{238}U, suggests a quadrupole resonance in the photofission, located at 9 MeV, in agreement with the expected $58A^{-1/3}$ MeV dependence for the resonance peak. The integrated photo cross section of this $E2$ resonance is 1.3% of the $E1$.

To summarize, even though our results allow only a small quadrupole strength in the transitions of the photonuclear giant resonance, this is in agreement with what is expected from sum rules arguments and other experimental evidence.

We acknowledge Professor J. Goldemberg, Professor D. S. Onley, and Professor W. C. Barber for useful discussions.

*Supported by Funcação de Amparo à Pesquisa do Estado de São Paulo—FAPESP.

[1]Nuclear size can be neglected when $kR \ll 1$, where R is the nuclear radius and k is the wave number of the momentum transfer. When one looks to the total cross section (see Ref. 3), in the giant resonance region, this condition is valid.

[2]J. A. Thie, C. J. Mullin, and E. Guth, Phys. Rev. 87, 962 (1952).

[3]W. W. Gargaro and D. S. Onley, Phys. Rev. C 4, 1032 (1971).

[4]K. L. Brown and R. W. Wilson, Phys. Rev. 93, 443 (1954).

[5]M. B. Scott, A. O. Hanson, and D. W. Kerst, Phys. Rev. 100, 209 (1956).

[6]R. L. Hines, Phys. Rev. 105, 1534 (1957).

[7]W. C. Barber, Phys. Rev. 111, 1642 (1958).

[8]W. C. Barber and T. Wiedling, Nucl. Phys. 18, 575 (1960).

[9]E. Wolynec, G. Moscati, O. D. Gonçalves, and M. N. Martins, Univ. de São Paulo Report No. IFUSP/P-38 (unpublished).

[10]This is a standard mode of operation in which the number of pulses arriving in each time interval is stored in successive channels.

[11]Bremsstrahlung which activates the back target is produced not only in the actual radiator but also in the front target and in the back target itself. This contribution is taken into account by considering an effective radiator whose thickness is $t_{\text{eff}} = [h\frac{3}{2}\, t_t + t_r]$, where $h \cong [Z_t(Z_t+1)A_r]/[Z_r(Z_r+1)A_t]$. Then, ht_t is the thickness of a radiator of atomic mass A_r and atomic number Z_r equivalent to a radiator of thickness t_t, atomic mass A_t, and atomic number Z_t.

[12]H. W. Koch and J. W. Motz, Rev. Mod. Phys. 31, 920 (1959).

[13]E. Wolynec, D. S. Onley, and I. Nascimento, Univ. de São Paulo Report No. IFUSP/P-42 (unpublished).

[14]J. D. King, R. N. H. Haslam, and W. J. McDonald, Can. J. Phys. 38, 1060 (1960).

[15]S. C. Fultz, J. T. Caldwell, B. L. Berman, R. L. Bramblett, and R. R. Harvey, Phys. Rev. 143, 790 (1966).

[16]S. C. Fultz, R. L. Bramblett, J. T. Caldwell, and P. R. Harvey, Phys. Rev. 133, B1149 (1964).

[17]F. Ferrero, S. Ferroni, R. Malvano, S. Menardi, and E. Silva, Nuovo Cimento 11, 410 (1959).

[18]A. Bohr and B. R. Mottelson, *Nuclear Structure* (Benjamin, New York, 1972), Vol. 2.

[19]R. Pitthan and T. Walcher, Phys. Lett. 36B, 563 (1971); Z. Naturforsch. 27a, 1863 (1972).

[20]M. B. Lewis, Phys. Rev. Lett. 29, 1257 (1972).

[21]M. B. Lewis and F. E. Bertrand, Nucl. Phys. A196, 337 (1972).

[22]S. Fukada and Y. Torizuka, Phys. Rev. Lett. 29, 1109 (1972).

[23]N. Nagao and Y. Torizuka, Phys. Rev. Lett. 30, 1068 (1973).

[24]R. Pitthan, F. R. Buskirk, E. B. Dally, J. N. Dyer, and X. K. Maruyama, Phys. Rev. Lett. 33, 849 (1974).

[25]V. L. Telegdi and M. Gell-Mann, Phys. Rev. 91, 169 (1953).

[26]J. S. O'Connell, in *Proceedings of the International Conference on Photonuclear Reactions and Applications, Asilomar, 1973,* edited by B. L. Berman (Lawrence Livermore Laboratory, Univ. of California, 1973), Vol. 1, A71, CONF-730301.

[27]J. D. T. Arruda Neto, M.Sc. thesis, Universidade de São Paulo, 1974 (unpublished); J. D. T. Arruda Neto, S. B. Herdade, and I. C. Nascimento, unpublished.